Aromatic Side Chain−Porphyrin Interactions in Designed Hemoproteins

Dahui Liu, David A. Williamson, Michelle L. Kennedy, Todd D. Williams,[†] Martha M. Morton,[‡] and David R. Benson*[,1]

Contribution from the Department of Chemistry, University of Kansas, Lawrence, Kansas 66045-0046

Received February 24, 1999. Revised Manuscript Received August 4, 1999

Abstract: Aromatic amino acid side chains are commonly observed to interact with the heme cofactors of natural hemoproteins. These interactions are of the types previously identified for pairs or groups of aromatic amino acid side chains in proteins: offset π-stacking and T-stacking (an edge-to-face arrangement). To evaluate how such interactions may influence structural stability of hemoproteins, we synthesized peptide-sandwiched mesohemes (PSMs) **2** and **3** in which the alanine-4 (Ala-4) residues in **1** have been replaced by phenylalanine (Phe) and tryptophan (Trp), respectively. The Co(III) analogues of **1**, **2,** and **3** (**1-Co**, **2-Co**, and **3-Co**, respectively) were also prepared. Histidine (His)-to-iron coordination in **1** had previously been shown to induce helical conformations in the peptides (helix content ∼50% at 8 °C). Molecular modeling studies suggested that Trp, but not Phe, could engage in edge-to-face interactions with the porphyrin if the peptides are fully helical. Replacing Ala-4 with Trp, but not with Phe, was thus predicted to favor enhanced peptide helix content. Circular dichroism spectra are consistent with significantly increased helix content in **3** relative to **1**, but not in **2**. Hydrogen−deuterium (H/D) exchange rates determined by electrospray ionization mass spectrometry, however, decrease in the order **1** ≫ **2** > **3**, while pH titrations reveal that the stability of the model protein folds decreases in the order **3** > **2** ≫ **1**. Furthermore, ^{1}H NMR spectra of **2-Co** and **3-Co** indicate that the aromatic side chains in each compound are oriented within the shielding region of the porphyrin ring. Two-dimensional NOE and chemical shift data show that the helices in **3-Co** are more highly organized than in **1-Co** and span nearly the entire peptide sequence, while in **2-Co** shorter helices of intermediate stability run between Phe-4 and Ala-13. The combined results indicate that aromatic side chain-porphyrin interactions in **2** and **3** stabilize their respective model protein folds, and suggest a similar role for the corresponding interactions in natural hemoproteins. Finally, the chemical shift patterns of the Trp side chains in **3-Co**, the different effects of Phe and Trp on peptide architecture, and the pattern of chemical shifts exhibited by the α-NH and α-CH hydrogens in all three Co(III) PSMs demonstrate that the solution structures of these designed hemoproteins are similar to those predicted in molecular modeling studies.

Introduction

London dispersion forces (induced dipole−induced dipole) are the major enthalpically stabilizing interactions between aliphatic amino acid side chains in the interiors of folded proteins.[2] For the case of two aromatic amino acid side chains in van der Waals contact with one another, an additional electrostatic component must be considered.[2,3] Electrostatic stabilization arises when hydrogen atoms on one aromatic ring (which bear a partial positive charge) lie above the π electrons of a second aromatic group. This can be accomplished when the two rings are oriented parallel to one another and offset (offset π-stacking), at right angles (a T-stacking or edge-to-face arrangement) or any angle in between. Calculations by Jorgenson and Severance have shown that for the benzene dimer, the T-stacking arrangement is more stable than the offset π-stacking by ∼0.2 kcal mol^{-1} (−2.31 vs −2.11 kcal mole^{-1}).[4] Although T-stacking includes an attractive Coulombic term, the interaction is dominated by the $1/r^6$van der Waals (London dispersion) term. This conclusion has recently received experimental support from Wilcox and co-workers.[5]

In a 1985 study involving 34 proteins, Burley and Petsko found that 60% of aromatic side chains are involved in aromatic−aromatic interactions of the types noted above.[6] T-stacking was found to predominate. Furthermore, a large percentage of aromatic side chains are involved in "networks" comprising three or more aromatic rings engaged in mutually stabilizing interactions. It was suggested that these networks could serve as nucleation points for protein folding.[6]

Interactions between heme and apolar amino acid side chains in the heme binding pocket are recognized as contributing to the structural stability of hemoglobin (Hb),[7] myoglobin (Mb),[8] cytochrome b_5[9] and cytochrome b_{562}.[10] Recent work has demonstrated that they are also largely responsible for apoMb's

[†] University of Kansas Mass Spectrometry Laboratory.
[‡] University of Kansas NMR Laboratory.
(1) Telephone: 785-864-4090. Fax: 785-864-5396. E-mail: drb@ukans.edu.

(2) Makhatadze, G. I.; Privalov, P. L. *Adv. Protein Chem.* **1995**, *47*, 307−425. (b) Honig, B.; Yang, A.-S. *Adv. Protein Chem.* **1995**, *46*, 27−58.

(3) Hunter, C. A.; Sanders, J. K. M. *J. Am. Chem. Soc.* **1990**, *112*, 5525−5534.

(4) Jorgensen, W. L.; Severance, D. L. *J. Am. Chem. Soc.* **1990**, *112*, 4768−4774.

(5) Kim, E.; Paliwal, S.; Wilcox, C. S. *J. Am. Chem. Soc.* **1998**, *120*, 11192−11193.

(6) (a) Burley, S. K.; Petsko, G. A. *J. Am. Chem. Soc.* **1986**, *108*, 7995−8001. (b) Burley, S. K. Petsko, G. A. *Adv. Protein Chem.* **1988**, *39*, 125−189.

(7) Leutzinger, Y.; Beychok, S. *Proc. Natl. Acad. Sci. U.S.A.* **1981**, *78*, 780−784.

(8) Hughson, F. M.; Baldwin, R. L. *Biochemistry* **1989**, *28*, 4415−4422.

10.1021/ja990606r CCC: $18.00
Published on Web 12/07/1999

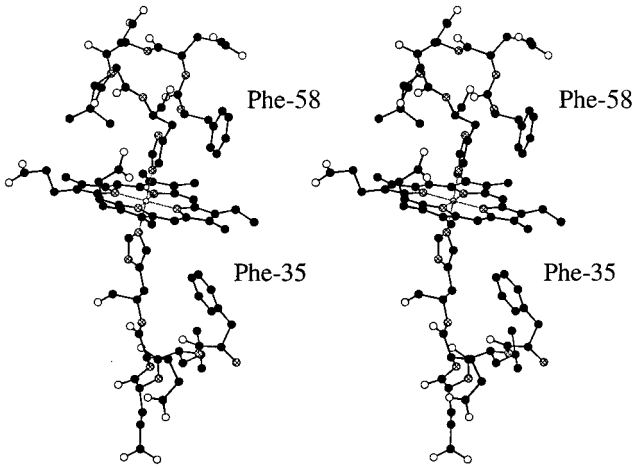

Figure 1. The heme binding pocket of bovine cytochrome b_5,[12] highlighting the interactions betweeen heme and Phe residues 35 and 58. Atom colors are as follows: carbon (black); oxygen (white); nitrogen (gray).

affinity for heme.[11] Our interest in the factors contributing to hemoprotein stability prompted us to examine the available hemoprotein structures in the Protein Data Bank. We were intrigued to discover that in the majority of hemoprotein structures reported to date, at least one phenylalanine (Phe), tryptophan (Trp), tyrosine (Tyr), or histidine (His) aromatic side chain is involved in either a π-stacking or a T-stacking interaction with the heme. Examples relevant to the present work include the invariant residues Phe-35 and Phe-58 of cytochrome b_5,[12,13] which are engaged in T-stacking interactions on opposite faces of the heme (Figure 1), and Trp-51 and Trp-191 of cytocohrome *c* peroxidase[14] and other Type-I plant peroxidases,[15] one of which is involved in a π-stacking interaction with the heme, the other in an edge-to-face interaction on the other side of the heme (Figure 2). A systematic study of aromatic side chain−heme interactions in all known hemoprotein crystal structures is currently underway and will be published separately.

Another common feature of hemoproteins is high α-helix content in the vicinity of the heme binding pocket. Hemoproteins exhibiting high helix content include the globins,[16] peroxidases,[14,15] catalases,[15] and the cytochromes *c*,[13a,17] b_5,[12,13] b_{562}, and P450.[18] A rare exception is nitrophorin,[19] an NO-transporting protein from blood-sucking insects, wherein the heme binding pocket is composed entirely of antiparallel β-sheet. A number of hemoprotein model systems containing helical peptides have also been designed. These include: (1) four-helix bundles in which each peptide is covalently attached to a "corner" of a porphyrin scaffold and in which the bundle is oriented perpendicular to the porphyrin plane,[20] (2) preformed four-helix bundles which bind one[21] or more[22] metalloporphyrins via bis-His coordination, (3) disulfide-dimerized peptides which bind a single metalloporphyrin via bis-His coordination,[23] (4) reversible complexes formed between a water-soluble Fe(III) porphyrin and amphiphilic peptides bearing centrally located His residues,[24] (5) porphyrin-spanning peptides either covalently attached[25] or bound via metal-to-ligand coordination[26] to *meso*-phenyl rings, and (6) bis-peptide adducts of metalloporphyrins in which His ligands within each peptide coordinate to the porphyrin-bound metal ion.[27,28] This sixth group of models comprises the peptide-sandwiched mesohemes (PSMs; e.g. **1**−**4**), developed in our laboratory,[27] and the closely related mimochromes, reported by Pavone and co-workers.[28]

In PSM **1**, two identical peptides are attached to iron(III) mesoporphyrin-II via amide linkages between the side chain of lysine-12 (Lys-12) and the propionate groups of the porphyrin.[29] Coordination of His-8 to iron induces the peptides to adopt conformations with ∼50% helix content in aqueous solution at 8 °C, as determined by circular dichroism (CD) spectroscopy.[29] Molecular modeling studies of **1** suggested that a fully helical peptide would adopt an orientation in which the helix axis lies at an angle of ∼30° relative to the heme plane, a result of the prediction that the His side chains would prefer torsional angles $\chi_1 = 180°$ and $\chi_2 = -90°$ due to the location of the Lys linker relative to His.[27b] Modeling studies further suggested that replacing alanine-4 (Ala-4) by Trp should permit edge-to-face interactions between the Trp side chain and the porphyrin in **3** if the peptides are fully helical.[29b] The side chain of Phe, in contrast, is predicted to be too small to permit the same kind of interactions in **2**. Herein we report the results of CD spectroscopy, hydrogen−deuterium exchange experiments, and pH titrations of **1**−**3**, as well as NMR studies of their Co(III) analogues, which reveal that the Phe side chains in **2** and the Trp side chains in **3** stabilize their respective folds. However, only in **3** do the aromatic side chain−porphyrin interactions

(9) (a) Falzone, C. J.; Mayer, M. R.; Whiteman, E. L.; Moore, C. D.; Lecomte, J. T. J. *Biochemistry* **1996**, *35*, 6519−6526. (b) Storch, E. M.; Daggett, V. *Biochemistry* **1996**, *35*, 11596−11604.

(10) (a) Arnesano, F.; Banci, L.; Bertini, I.; Faraone-Mennella, J.; Rosato, A.; Barker, P. D.; Fersht, A. R. *Biochemistry* **1999**, *38*, 8657−8670. (b) Feng, Y.; Sligar, S. G. *Biochemistry* **1991**, *30*, 0, 10150−10155.

(11) Hargrove, M. S.; Wilkinson, A. J.; Olson, J. S. *Biochemistry* **1996**, *35*, 11300−11309.

(12) Mathews, F. S.; Argos, P.; Levine, M. *Cold Spring Harbor Symp. Quantum Biol.* **1972**, *36*, 387 (PDB accession code 1CYO).

(13) (a) Mathews, F. S. *Prog. Biophys. Mol. Biol.* **1985**, *45*, 1−56. (b) Ozols, J.; *Biochim. Biophys. Acta* **1989**, *997*, 121−130.

(14) Goodin, D. B.; McRee, D. E. *Biochemistry* **1993**, *32*, 3313−3324 (PDB accession code 1CCA).

(15) Dunford, H. B. *Heme Peroxidases*; Wiley-VCH: New York, 1999.

(16) (a) Bashford, D.; Chothia, C.; Lesk, A. M. *J. Mol. Biol.* **1987**, *196*, 199−216. (b) Lesk, A. M.; Chothia, C. *J. Mol. Biol.* **1980**, *136*, 225−270.

(17) Moore, G. R.; Pettigrew, G. W. *Cytochromes c: Evolutionary, Structural and Physicochemical Aspects*; Springer-Verlag: Berlin, 1990; Chapters 4 and 5.

(18) Ortiz de Montellano, P. R. *Cytochrome P450: Structure, Mechanism and Biochemistry*, 2nd ed.; Plenum: New York,

(19) Weichsel, A.; Andersen, J. F.; Champagne, D. E.; Walker, F. A.; Montfort, W. R. *Nat. Struct. Biol.* **1998**, *5*, 304−309.

(20) (a) Sasaki, T.; Kaiser, E. T. *J. Am. Chem. Soc.* **1989**, *111*, 380−381. (b) Akerfeldt, K. S.; Kim, R. M.; Camac, D.; Groves, J. T.; Lear, J. D.; DeGrado, W. F. *J. Am. Chem. Soc.* **1992**, *114*, 9656−9657. (c) Mihara, H.; Tomizaki, K.-y.; Fujimoto, T.; Sakamoto, S.; Aoyagi, H.; Nishino, N. *Chem. Lett.* **1996**, 187−188.

(21) (a) Choma, C. T.; Lear, J. D.; Nelson, M. J.; Dutton, P. L.; Robertson, D. E.; DeGrado, W. F. *J. Am. Chem. Soc.* **1994**, *116*, 856−865. (b) Rau, H. K.; Haehnel, W. *J. Am. Chem. Soc.* **1998**, *120*, 468−476.

(22) Robertson, D. E.; Farid, R. S.; Moser, C. C.; Urbauer, J. L.; Mulholland, S. E.; Pidikiti, R.; Lear, J. D.; Wand, A. J.; DeGrado, W. F.; Dutton, P. L. *Nature* **1994**, *368*, 425−432.

(23) (a) Arnold, P. A.; Shelton, W. R.; Benson, D. R. *J. Am. Chem. Soc.* **1997**, *119*, 3181−3182. (b) Sakamoto, S.; Ueno, A.; Mihara, H. *J. Chem. Soc., Perkin Trans. 2* **1998**, 2395−2404.

(24) Huffman, D. L.; Rosenblatt, M. M.; Suslick, K. S. *J. Am. Chem. Soc.* **1998**, *120*, 6183−6184.

(25) Geier III, G. R.; Sasaki, T. *Tetrahedron Lett.* **1997**, *38*, 3821−3824.

(26) Karpishin, T. B.; Vannelli, T. A.; Glover, K. J. *J. Am. Chem. Soc.* **1997**, *119*, 9063−9064.

(27) (a) Benson, D. R.; Hart, B. R.; Zu, X.; Doughty, M. B. *J. Am. Chem. Soc.* **1995**, *117*, 8502- 8510. (b) Arnold, P. A.; Benson, D. R.; Brink, D. J.; Hendrich, M. P.; Jas, G. S.; Kennedy, M. L.; Petasis, D. T.; Wang, M. *Inorg. Chem.* **1997**, *36*, 5306−5315. (c) Liu, D.; Lee, K.-H.; Benson, D. R. *Chem. Commun.* **1999**, 1205−1206.

(28) (a) Nastri, F.; Lombardi, A.; Morelli, G.; Maglio, O.; D'Auria, G.; Pedone, C.; Pavone, V. *Chem. Eur. J.* **1997**, *3*, 340−349. (b) D'Auria, G.; Maglio, O.; Nastri, F.; Lombardi, A.; Mazzeo, M.; Morelli, G.; Paolillo, L.; Pedone, C.; Pavone, V. *Chem. Eur. J.* **1997**, *3*, 350−362.

(29) (a) Wang, M.; Kennedy, M. L.; Hart, B. R.; Benson, D. R. *Chem. Commun.* **1997**, 883−884. (b) Williamson, D. A.; Benson, D. R. *Chem. Commun.* **1998**, 961−962.

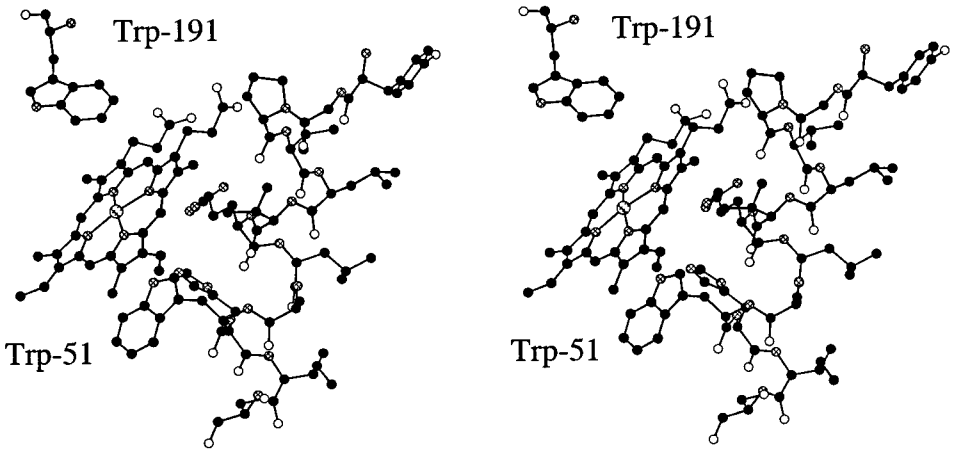

Figure 2. The heme binding pocket of bovine cytochrome *c* peroxidase,[14] highlighting the interactions betweeen heme and Trp residues 51 and 191. Atom colors as in Figure 1.

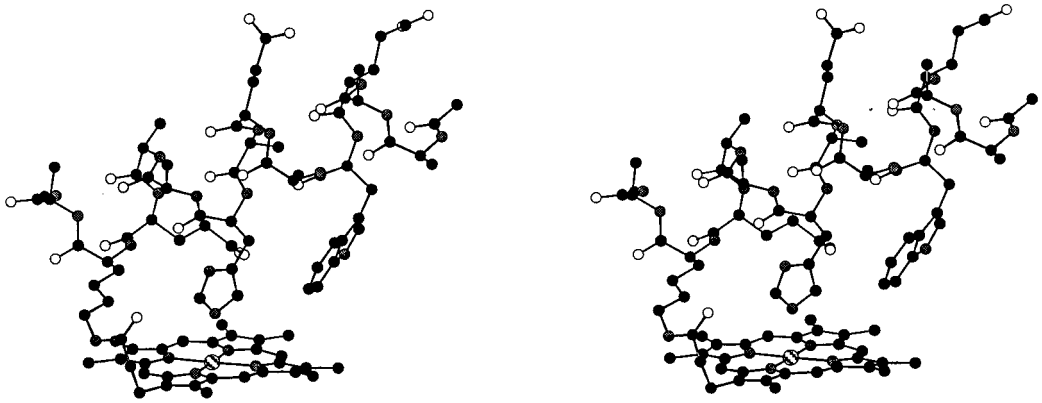

Figure 3. Structure of **3** predicted by molecular modeling. Only one peptide is shown. Atom colors as in Figure 1.

support a full-length helix. Our results suggest that aromatic side chain−heme interactions in natural hemoproteins may be important for maintaining high affinity for heme and for stabilizing the hemoprotein folds.

Results and Discussion

Design and Synthesis. Molecular modeling studies for the MP-IX analogue of **1** have been reported previously (the compound was designated as **2** in that paper).[27b] In those studies we found that the His side chain torsional angle combination $\chi_1/\chi_2 \approx 180°/-90°$ was likely to be favored over the only other reasonable combination ($\chi_1/\chi_2 \approx -60°/90°$) due to constraints imposed by the location of the Lys linker relative to His. A model of **1** was generated from the MP−IX structure by deleting the bond connecting one of the propionate groups to the porphyrin, rotating about the Fe−His bond, reconnecting the propionate group to the porphyrin at the appropriate position, and performing an energy minimization.[30] Ala-4 was then converted to either Phe or Trp. All possible combinations of ideal side chain torsional angles χ_1 (−60°, +60°, 180°) and χ_2 (−90°, +90°)[31] were examined in order to determine whether edge-to-face interactions between the side chain and the porphyrin were possible. For **3**, only side chain torsional angles $\chi_1/\chi_2 = 180°/-90°$ pointed the indole ring toward the porphyrin. Energy minimization of this structure led to the molecule shown in Figure 3. For **2**, Phe side chain torsional angles $\chi_1/\chi_2 = 180°/-90°$ also directed the phenyl ring toward the porphyrin, but the distance separating the two was larger, as expected based upon the relative sizes of the Trp and Phe side chains. Molecular modeling studies showed that if the His side chain torsional angle combination $\chi_1/\chi_2 = -60°/90°$ were adopted instead, the peptide helix axis would be parallel to the porphyrin plane and both Trp and Phe would be capable of engaging in T-stacking interactions with the porphyrin.

Synthesis of **1**−**4** commences with the bis-*p*-nitrophenyl ester of iron(III) MP-II, which is prepared by insertion of iron into the bis *p*-nitrophenyl ester of the free base porphyrin.[29a] This is followed by reaction with the appropriate peptide in DMSO in the presence of excess diisopropylethylamine (DIEA). Syntheses

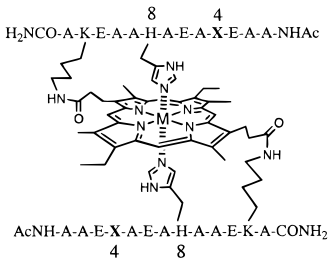

1: M = Fe(III); X = Ala
2: M = Fe(III); X = Phe
3: M = Fe(III); X = Trp
4: M = Fe(III); X = p-F-Phe

1-Co: M = Co(III); X = Ala
2-Co: M = Co(III); X = Phe
3-Co: M = Co(III); X = Trp

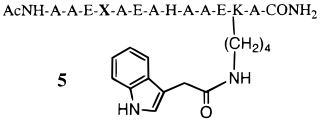

(30) Sybyl molecular modeling software version 6.5, Tripos Associates, Inc., St. Louis, MO.

(31) McGregor, M. J.; Islam, S. A.; Sternberg, M. J. E. *J. Mol. Biol.* **1987**, *198*, 295−310.

of the Co(III) PSMs required an alternative route, as attempts at inserting cobalt into the bis-*p*-nitrophenyl ester of MP-II were unsuccessful. Thus the bis-*p*-nitrophenyl ester of MP-II is treated with 4 equiv of peptide and 10 equiv of DIEA in the presence of excess $Co(Ac)_2$. Purification in all cases is achieved by sequential ion exchange chromatography, reversed phase HPLC, and gel filtration.

Concentration Studies with 4. Porphyrins and metalloporphyrins aggregate strongly in aqueous solution.[33] Although the presence of peptides on both faces of the porphyrin in **1**−**3** and their Co(III) analogues should mitigate this problem, exposed hydrophobic surfaces may still lead to self-association at high concentration. NMR provides a useful means of analyzing aggregation behavior, as NMR chemical shifts and line shapes are highly sensitive to environment. We have studied the *p*-fluorophenylalanine analogue of **2** (**4**) for this purpose, using ^{19}F NMR.

^{19}F NMR spectra of **4** were measured at concentrations ranging from 50 μM to >1 mM in water and in 3:1 H_2O/CH_3OH, both buffered to pH 7.0. Two signals of equal intensity were observed (Figure S1, Supporting Information), consistent with expectations that the two peptides in **4** (and in the other PSMs) differ in their orientation relative to the porphyrin. At 1 mM in aqueous solution the peaks were broad and overlapping, but the signals sharpened significantly as concentration was lowered (Figure S1). Between 1 mM and about 135 μM, the chemical shifts of the two signals changed substantially as well, relative to the internal NaF standard. The difference in chemical shifts of the two signals is shown plotted vs the natural log of the concentration in Figure S2 (Supporting Information). Below ~135 μM, no further concentration dependent changes were observed. This suggests that the PSMs are monomeric at the low concentrations (4−6 μM) used for measuring UV/vis and CD spectra in aqueous solution. In 3:1 H_2O/CH_3OH (pH 7), chemical shifts and line shapes of the two signals were constant over the entire concentration range studied (Figure S2), providing strong evidence that **1**−**3** will be monomeric in this solvent under the conditions used in the H/D exchange and pH titration experiments discussed in later sections.

Ultraviolet/visible Spectroscopy. UV/vis spectra of Fe(III)-PSMs **1**−**3** in water, in 3:1 (v/v) H_2O/1-propanol, and in 3:1 (v/v) H_2O/methanol, all buffered to pH 7 with 2 mM potassium phosphate indicate that the iron atom is low-spin, consistent with bis-His coordination[32] (spectra not shown). The Soret band λ_{max} for **1**, **2,** and **3** in water is 402.2, 403.2, and 404.1 nm, respectively, while the β (Q_v) and α (Q_o) bands for each compound are centered near 525 and 565 nm, respectively. The Soret band extinction coefficients of **1**−**3** are all ~130 000 $M^{-1}cm^{-1}$ in neutral aqueous solution. Absence of significant high spin iron(III) in **1**−**3** is indicated by lack of π-iron charge-transfer bands near 620 nm and by small or unobservable high-spin signals in EPR spectra.[34] UV/vis spectra of Co(III) analogues in neutral aqueous solution are also consistent with bis-His coordination. The Soret band λ_{max} is 417.2 nm (ϵ = 180 000 $M^{-1}cm^{-1}$) for each, while the β and α bands are centered near 526 and 562 nm, respectively.

Circular Dichroism Studies of 1−3. Because water can compete for hydrogen bonding to peptide backbone amides, it is an unfavorable medium for achieving helical conformations in peptides. As a means of evaluating the success of a particular hemoprotein design incorporating helical peptides, we therefore routinely record circular dichroism (CD) spectra in aqueous solution. CD spectra of **1**−**3**, 5 μM in 2 mM potassium phosphate buffer (pH 7.0) are shown in Figure 4 (spectra of the Co(III) analogues are nearly identical; data not shown). Each spectrum exhibits features characteristic of α-helical structure, including a minimum corresponding to the amide $n-\pi^*$ transitions centered near 220 nm, and a minimum near 208 nm and a maximum near 195 nm resulting from exciton-coupled amide $\pi-\pi^*$ transitions.[35] Spectra of **1**−**3** diluted 10-fold are unchanged (not shown), supporting the results of ^{19}F experiments with **4** which indicate that the compounds are monomeric under these conditions. Assuming that the peptides are in a simple helix−coil equilibrium, and that no other chromophores contribute to the spectrum, the fraction of amino acids occupying helical conformations (*f*) can be calculated from the mean residue ellipticity (MRE) at 220 nm (θ_{220}) using eqs 1[36] and 2,[37] where $\theta_\infty = -40\,000$ deg·cm^2 dmol^{-1}, $\theta_0 = -1500$ deg·cm^2 dmol^{-1} (determined from the CD spectrum of **5**) and $n = 26$. Helix constants estimated using θ_{220} in water are listed in Table 1.

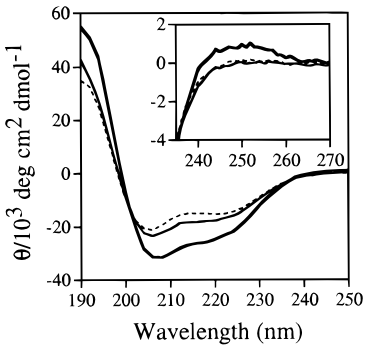

Figure 4. CD spectra of **1** (dashed line), **2** (thin solid line), and **3** (bold solid line) in 2 mM pH 7 potassium phosphate buffer at 8 °C.

Table 1. CD Data for **1**−**3**

	H_2O (8 °C)		25% PrOH (8 °C)		25% MeOH(25 °C)	
PSM	$-\theta_{220}$	*f* (%)	$-\theta_{220}$	*f* (%)	$-\theta_{220}$	*f* (%)
1	13800	50	21400	77	15400	56
2	16200	58	24400	88	17000	61
3	23100	83	26400	95	23100	83

$$f = (\theta_{obs} - \theta_0)/(\theta_{max} - \theta_0) \quad (1)$$

$$\theta_{max} = \theta_\infty[(n-4)/n] \quad (2)$$

The CD data suggest that helix content in **3** is much higher than in **1**. Furthermore, helix content of **2** does not appear to be significantly increased relative to **1**. Both results match our predictions from molecular modeling. However, as discussed below, aromatic amino acids and heme can both contribute to CD spectra in the far-UV region, making the data in Table 1 suspect. We therefore investigated the effect of the helix-stabilizing cosolvent PrOH on CD spectra of **1**−**3** to provide further evidence for the relative helix contents indicated in the aqueous spectra (Figure 5; ellipticity data for **1**−**3** in 3:1 (v/v)

(32) Adar, F. In *The Porphyrins*; Dolphin, D., Ed.; Academic: New York, 1978; Vol. 3, Chapter 2.

(33) (a) Kolski, G. B.; Plane, R. A. *J. Am. Chem. Soc.* **1972**, *94*, 3740−3744. (b) Pasternack, R. F. *Ann. N.Y. Acad. Sci.* **1973**, *206*, 614−630.

(34) Kennedy, M. L.; Gibney, B. R.; Dutton,. P. L.; Rodgers, K. R.; Benson, D. R. *J. Am. Chem. Soc.*, manuscript submitted for publication.

(35) Woody, R. W.; Dunker, A. K. In *Circular Dichroism and the Conformational Analysis of Biomolecules*; Fasman, G. D., Ed.; Plenum: New York, 1996; Chapter 4.

(36) Chang, C. T.; Wu, C.-S. C.; Yang, J. T. *Anal. Biochem.* **1978**, *91*, 13−31.

(37) Lyu, P. C.; Sherman, J. C.; Chen, A.; Kallenbach, N. R. *Proc. Natl. Acad. Sci. U.S.A.* **1991**, *88*, 5317−5320.

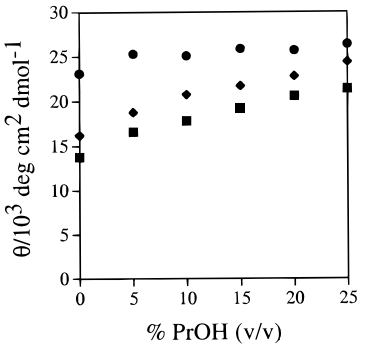

Figure 5. θ_{220} as a function of PrOH concentration for **1** (■), **2** (◆), and **3** (●). All samples are buffered to pH 7 with 2 mM potassium phosphate.

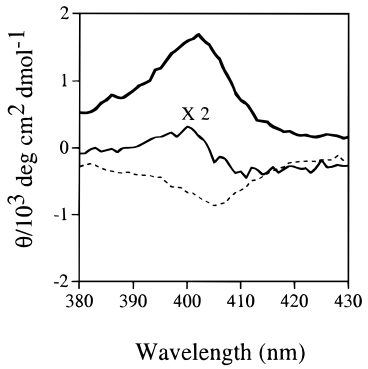

Figure 6. Soret region CD spectra of **1**−**3** in 2 mM pH 7 potassium phosphate buffer at 8 °C.

H_2O/PrOH at 8 °C are shown in Table 1). We found that for **3**, maximum helix content is achieved in the presence of only 5−10 volume % PrOH, confirming that helix content in water is already very high. In contrast, θ_{220} for **1** and **2** has not leveled off even at 25 volume % PrOH (Figure 5), indicating much lower helix content in both compounds in aqueous solution. Furthermore, plots of $-\theta_{220}$ vs volume % PrOH for **1** and **2** are quite similar, the only difference being that $-\theta_{220}$ for **2** is slightly larger throughout. Close inspection of the spectra of **1** and **2** in aqueous solution reveal some differences, however. For instance, the low wavelength minima of **1** and **2** are centered at 206 and 207 nm, respectively. In addition, the shapes of the spectra are slightly different, particularly in the region between 220 and 208 nm.

Contributions to far-UV CD spectra are commonly encountered in peptides[35,38] and proteins[35] containing aromatic amino acids, particularly Trp and Tyr, both of which absorb strongly in the far-UV region. The signals result from coupling between the $\pi-\pi^*$ electric dipole transition moments of the aromatic side chain and the peptide backbone amides,[34] and can lead to significant errors in peptide helix content measured using eq 1.[38] Baldwin and co-workers found by using difference-CD spectroscopy that Trp contributes negative ellipticity to CD spectra of monomeric peptides, which leads to an overestimation of peptide helix content.[38] A correction for Trp can thus be made in suitable cases. However, the CD spectrum of **3** exhibits *increased* ellipticity relative to **1** and **2** between 240 and 260 nm (Figure 4, inset), which is not observed in the difference CD spectra of Baldwin and co-workers,[38] indicating that the contribution from Trp in **3** may in fact be quite different in our hemoprotein models. The factor that differentiates **3** from the Baldwin peptides is that the porphyrin chromophore can generate signals in far-UV CD spectra as well,[39] via coupling of its transition dipoles with those of the peptide backbone amides and/or aromatic side chains in the peptides. The positive signal between 240 and 260 nm in the spectrum of **3**, which is also present in spectra measured in 1:1 H_2O/CH_3OH, is absent in pure CH_3OH. Loss of the positive signal in **3** upon changing the solvent from H_2O to CH_3OH suggested a reduction of Trp−porphyrin interactions, a hypothesis that is supported by ^1H NMR data (vide infra). This observation indicates that the positive signal in the more polar solvent arises primarily from coupling between the Trp and porphyrin transition dipoles. If one assumes a Gaussian shape for this Trp-induced band, it would thus contribute a small amount of *positive* ellipticity at 220 nm. Thus, a simple correction of the CD data of **3** based on Baldwin's results is not justified.

Hemoproteins[40] and peptide−metalloporphyrin adducts[27,28,41] and complexes[23,42] commonly exhibit CD signals in the Soret region (spectra for **1**−**3** are shown in Figure 6). The heme Soret band arises from two nearly degenerate $\pi-\pi^*$ electronic transitions (B_x and B_y) which are in the porphyrin plane and polarized perpendicularly to one another.[39] The absence of an aromatic side chain in **1** demonstrates that its CD Soret signal arises primarily from coupling of these heme transition dipoles with those of the peptide backbone amides (see discussion in ref 27a). In **2** and **3**, both the peptide backbone amides and the aromatic side chains can contribute. Interestingly, the shape of the Soret band is different for each compound. Although the intensities of the signals change as a function of peptide helix content (varied by adding PrOH; not shown), their overall shapes remain the same. The differences in shape of the CD Soret spectra of **2** and **3** relative to **1** thus arise primarily from coupling between the aromatic side chains and the porphyrin. The bimodal shape of the CD Soret band for **2** shows that the contributions of B_x and B_y to the CD Soret band are of opposite sign.

In summary, although quantitative determination of helix content is complicated by the heme and aromatic side chain chromophores, the CD results strongly suggest that **1** and **2** have similar helix contents, while helix content in **3** is much higher. Although this result is consistent with predictions from molecular modeling, data presented in the next several sections indicate that the structural properties of **1** and **2** are in fact quite different.

Hydrogen−Deuterium Exchange Experiments. Peptide backbone amide hydrogens involved in hydrogen bonds are protected against exchange with D_2O.[43] Increased helix content

(38) Chakrabartty, A.; Kortemme, T.; Padmanabhan, S.; Baldwin, R. L. *Biochemistry* **1993**, *32*, 2, 5560−5565.

(39) Reviewed in: (a) Myer, Y. P.; Pande, A. In *The Porphyrins*; Dolphin, D., Ed.; Academic Press: New York, 1978; Volume 3, Chapter 6. (b) Myer, Y. P. *Methods Enzymol.* **1978**, *54*, 249- 284. (c) Hatano, M. *Adv. Polym. Sci.* **1986**, *77*, 1−135.

(40) (a) Nicola, N. A.; Minasian, E.; Appleby, C. A.; Leach, S. J. *Biochemistry* **1975**, *14*, 5141- 5149. (b) Zand, R.; Vinogradov, S. *Biochem. Biophys. Res. Commun.* **1967**, *26*, 121- 127. (c) Sugita, Y.; Dohi, Y.; Yoneyama, Y. *Biochem. Biophys. Res. Commun.* **1968**, *31*, 447−452. (d) Gersonde, K.; Sick, H.; Wollmer, A.; Buse, G. *Eur. J. Biochem.* **1972**, *25*, 181−189. (e) Shikama, K.; Suzuki, T.; Sugawara, Y.; Katagiri, T.; Takage, T.; Hatano, M. *Biochim. Biophys. Acta* **1982**, *701*, 138−141. (f) Hsu, M.-C.; Woody, R. W. *J. Am. Chem. Soc.* **1971**, *93*, 3515−3525.

(41) (a) Blauer, G.; Sreerama, N.; Woody, R. W. *Biochemistry* **1993**, *32*, 6674−6679 and references therein. (b) Okuyama, K.; Murakami, T.; Nozawa, T.; Hatano, M. *Chem. Lett.* **1982**, 111−114.

(42) (a) Blauer, G. *Nature (London)* **1961**, *189*, 396. (b) Blauer, G. *Biochim. Biophys. Acta* **1967**, *79*, 547. (c) Tsuchida, E.; Hasegawa, E.; Honda, K. *Biochim. Biophys. Acta* **1976**, *427*, 520−529.

(43) (a) Creighton, T. E. *Proteins: Structures and Molecular Properties*, 2nd ed.; Freeman: New York, 1993; pp 282−286. (b) Englander, S. W.; Kallenbach, N. R. *Q. Rev. Biophys.* **1983**, *16*, 521−655.

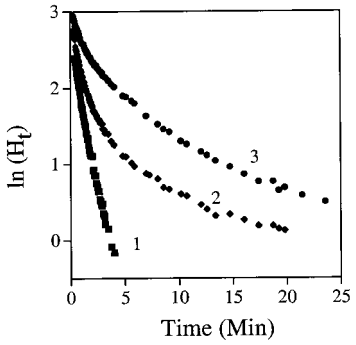

Figure 7. Data from H/D exchange experiments on **1** (■), **2** (◆) and **3** (●) plotted as ln(*Ht*) vs time. See text and Tables 2 and S1 for details.

in a peptide should thus lead to decreased rates of hydrogen−deuterium (H/D) exchange. Indeed, Anderegg and co-workers have shown using electrospray ionization mass spectrometry (ESI-MS) that backbone amide H/D exchange rates in 31-residue peptides correlate well with helix content.[44] We therefore undertook an investigation of H/D exchange in **1**−**3** as an additional means of evaluating the relative helix contents of the compounds.

H/D exchange experiments on **1**−**3** were performed via ESI-MS at 23 °C in 3:1 D_2O/CD_3OD, buffered to pD* 6.2 with 2 mM ammonium acetate. Under these conditions, the Fe(III) in **1**−**3** is predominantly bis-His coordinated as shown by pH titrations (vide infra), and the compounds are monomeric as shown in concentration studies using **4**. This solvent composition was chosen because at the temperatures used in the H/D exchange experiments, CD spectra closely match those measured in aqueous solution at 8 °C (Table 1, Figure 4 and Figure S3, Supporting Information). Ammonium acetate was used as a buffer to avoid diluting the ESI-MS signals by cation adduct formation, which occurs with the potassium phosphate buffers used in CD experiments (ammonium acetate cannot be used for CD spectra because of strong absorption of the buffer in the far-UV region). Finally, the pH chosen for the H/D exchange was lower than that in the CD experiments so as to slow the rate of exchange without measurably affecting Fe−His coordination as determined from pH titration data.

PSMs **1** and **2** contain a total of 34 exchangeable Hs: 32 amide NH hydrogens (26 from the peptide backbones, 4 from the C-terminal amides and 2 from the Lys side-chain amides) and 2 His side-chain NH hydrogens. The Trp side-chain NH hydrogens in **3** increase its total to 36. The six glutamic acid (Glu) residues will be deuterated during the electrospray process and thus will contribute to the observed mass increases. Total increases in mass for **1**, **2**, and **3** will thus be 40, 40, and 42, respectively.

Results for **1**−**3** are shown in Figure 7, plotted as ln(Ht) (Ht = the number of unexchanged hydrogens remaining) vs time. Curve-fitting using the linear regression method of Wagner et al.[44] yields two or more approximately linear regions for the compounds, each representing a group of amide hydrogens exchanging with similar rates. The fastest group cannot be measured directly and is determined from the difference between the number of observed exchangers and the total number that can exchange in each. Results of the curve-fitting (Figures S4−S6) are reported in Tables 2 and S1 (Supporting Information). The plot for **1** fits well to two distinct groups, while those for **2** and **3** fit best to four. Observed half-lives for exchange vary over more than an order of magnitude.

Table 2. Number of Hydrogens Exchanging over a Given Range of Half-Lives[a]

	$t_{1/2}$ (min)			
PSM	<0.5[b]	0.5−2	3−6	>9
1	21.1	18.9		
2	17.6	12.4	5.8	4.2
3	16.5	5.2	12.1	8.2

[a] See also Table S1 (Supporting Information). [b] Too fast to measure; determined by the difference between the total observed and the total number of exchangeable hydrogens (includes the Glu residues).

The most striking feature of the H/D exchange profiles is that **1** and **2** are so different from one another, even though their CD spectra are very much alike. In **1**, exchange is essentially complete within 5 min and occurs with a half-life of <1.08 min. In contrast, both **2** and **3** contain some hydrogens that exchange with half-lives of 11−12 min. These slowest exchangers number approximately 4 in **2** (∼2 per peptide) and 8 in **3** (∼4 per peptide). In **2**, 10 hydrogen atoms (5 in each peptide) exchange with half-lives longer than 3 min, whereas in **3** there are twice as many. The H/D exchange data clearly demonstrate that the aromatic side chains in both **2** and **3** alter peptide dynamics relative to **1**, even though the CD data indicate that helix contents in **1** and **2** are similar. On the basis of these results we postulated that the Phe side chains in **2** engage in stabilizing interactions with the porphyrin, but to a lesser extent than the Trp side chains in **3** and with different effects on peptide conformation. Stabilizing Phe−porphyrin interactions in **2** were subsequently confirmed in pH titrations (vide infra).

All of the observed exchange rates are remarkably slow for 13-residue peptides. H/D exchange results measured via ESI-MS by Stevenson et al. for a 15-residue peptide provide a useful comparison.[45] Under the experimental conditions used in their report (pH ≈ 3.5, 80% MeOH in water), peptide helix content is 80%, and the average half-life for exchange is 45 s (only the final 20% of exchange was observed). This is similar to the half-life observed for H/D exchange in **1**, which exhibits substantially lower helix content, at pH 6.2. An increase of one pH unit increases amide exchange by a factor of 10.[43] Thus, exchange is more than 2 orders of magnitude slower than might be expected if the dynamics of the two peptides are comparable. We propose that the slower exchange observed in the PSMs arises from the conformational constraints provided by the Fe−His bonds and the Lys−propionate linkers, which alter the dynamics of the helix−coil equilibrium relative to the unconstrained peptide studied by Stevenson et al.[45] The results suggest that in the PSM helix−coil equilibria, the rate of helix formation from the coil is rapid compared to the rate of deuterium exchange. In other words, exchange is of the most commonly observed EX_2 type.[43a]

We have noted that the two peptides in each PSM are oriented differently relative to the porphyrin macrocycle. We thus predicted that their conformational dynamics might also differ. Preliminary H/D exchange experiments using NMR have confirmed that the His backbone hydrogens on the two peptides in **3** exchange at unequal rates. Quantitative NMR H/D exchange studies of **2** and **3** are now underway, results of which will be reported in due course.

Finally, our results show that caution must be exercised when attributing differences in H/D exchange behavior of closely related peptides solely to changes in average peptide conformation as determined by CD. Conversely, they highlight the ability

(44) Wagner, D. S.; Melton, L. G.; Yan, Y.; Erickson, B. W.; Anderegg, R. J. *Protein Sci.* **1994**, *3*, 1305−1314.

(45) Stevenson, C. L.; Anderegg, R. J.; Borchardt, R. T. *J. Am. Soc. Mass Spectrom.* **1993**, *4*, 646−651.

of ESI-MS to expose structural differences between complex molecules that might otherwise be difficult to obtain in such a rapid manner.

pH titrations. At neutral pH, the high local concentration of the intramolecular His ligands in the PSMs strongly favors Fe−His coordination. Dissociation of the exchange-labile Fe−His bonds leads to unwinding of the helix and conversion of iron(III) from low spin to high spin. As pH is lowered, protonation of His becomes increasingly favored over coordination of His to Fe. Thus, pH titrations represent a way of comparing relative stabilities of the folded (bis-His coordinated) forms of PSMs such as **1**−**3**.

We have previously reported results of pH titrations for the MP-IX analogue of **1** (numbered **2** in that report) and for a group of isomeric PSMs having different His-Lys separations.[27b] In that work, we observed a modest dependence of pH midpoint on the distance separating His from the Lys linker (the smaller the separation, the greater the stability toward acid). For one pair of PSMs having equal His-Lys separation yet very different helix contents (≈5% vs 32%; compounds **3** and **4** in ref 27b), higher peptide-helix content was manifested in enhanced stability of the folded (bis-His coordinated) form of the molecule.

In the previously reported pH titrations, small deviations from isosbestic behavior were observed, which prevented us from obtaining accurate midpoint values.[27b] We attributed this to a combination of self-association in aqueous solution at low pH and the fact that the MP-IX PSMs exist in two interconverting diastereomeric forms. As noted in that report, midpoints obtained in pH titrations represent the product of the His protonation constants (K_{His}) and of the two individual Fe−His binding constants K_1 and K_2 [$(K_{His})^2K_1K_2$]. The fact that K_2 is generally much larger than K_1 makes accurate determination of K_1 and K_2 difficult.[46]

In the H/D exchange experiments, altered peptide dynamics in **2** and **3** relative to **1** suggested that both Phe and Trp are able to make stabilizing contacts with the porphyrin. We predicted that such interactions, if indeed present, would stabilize the folded forms of these compounds relative to the unfolded forms. We thus performed pH titrations on **1**−**3** using 3:1 H_2O/CH_3OH (23 °C) as solvent. This solvent was chosen to (1) maintain consistency with the H/D exchange work and (2) minimize self-association at lower pH, where the hydrophobic porphyrin is exposed to solvent. Isosbestic behavior was observed in all cases except at the lowest pHs for **2** and **3** (see Experimental Section). A representative titration of **1** is shown in Figure 8. The same data with curve-fitting results[47] are presented in Figure S7 (Supporting Information). Plots of Soret band extinction coefficient vs pH for **1**−**3** are shown in Figure 9. Midpoint values for **1**, **2,** and **3** are 3.82, 3.27, and 2.99, respectively. These data clearly show an increase in stability toward acid in the order **1** < **2** < **3**. The pH titration data convincingly demonstrate that the aromatic amino acid side chains stabilize the folded structures of both **2** and **3** relative to **1** and that the effect is more pronounced in the case of **3**.

1D NMR Studies of Aromatic Side Chain−Porphyrin Interactions. Bis-His coordinated Co(III) porphyrins are diamagnetic and exchange inert, and thus **1-Co**, **2-Co,** and **3-Co** are more amenable to ^{1}H NMR analysis[28b] than the paramagnetic Fe(III) PSMs or the extremely air-sensitive and exchange-labile diamagnetic Fe(II) analogues. One-dimensional ^{1}H NMR data

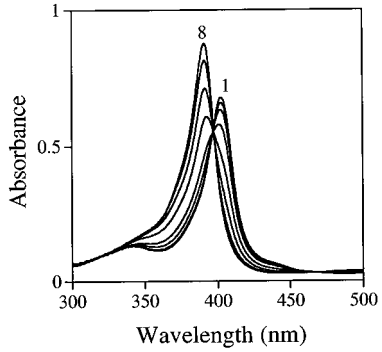

Figure 8. UV/vis spectra of **1** (7 μM) as a function of pH in 3:1 H_2O/CH_3OH, 23 °C. Spectrum 1: pH 5.51; Spectrum 8: pH 2.65.

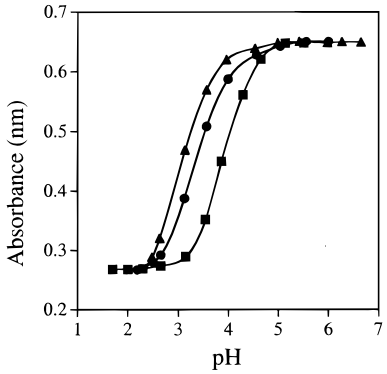

Figure 9. Plots of Soret band extinction coefficient vs pH for **1** (■), **2** (●), and **3** (◆). Spectra were recorded in 3:1 H_2O/CH_3OH at 23 °C. Sample concentrations ranged from 6 to 8 μM.

for **2-Co** and **3-Co** in CD_3OD are shown in Figure 10 (top spectrum). The only resonances downfield of 5 ppm in this solvent belong to the Trp and Phe side chains. As expected based on our NMR studies with **4**, the Trp and Phe residues in each peptide exhibit a separate set of signals (denoted throughout as unprimed for one peptide and primed for the other; e.g., H1 and H1′). Trp H1 and H1′ were tentatively identified in a 1D spectrum of **3-Co** in CD_3OH (not shown) based on their shape (a pair of singlets), their chemical shifts (9.69 and 9.82 ppm), and the fact that the signals disappear in CD_3OD. Observation of NOE signals between these protons and H2 and H2′ (also a pair of singlets, but which do not disappear in CD_3OD) confirmed their assignments. NOE signals between H1 and H1′ and the multiplets centered at 6.23 and 6.39 next identified those protons as H7 and H7′, respectively. The remaining protons were readily assigned from a COSY spectrum. The two sets of Phe side chain protons in **2-Co** were easily identified based on their multiplicity, integrals, and COSY data.

Figure 10 reveals that most of the Trp side chain protons in **3-Co** and Phe side chain protons in **2-Co** are shifted upfield relative to their normal positions. The strong upfield shifts support our conclusions from the H/D exchange and pH titration studies, which had suggested that the side chains of both Phe and Trp interact strongly with the porphyrin. Such interactions place the side chains within the shielding region of the porphyrin ring.[48]

Figure 10 also shows spectra of **2-Co** and **3-Co**, respectively, as increasing amounts of D_2O are added to a sample in CD_3OD. As the solvent is made increasingly polar, almost all of the aromatic side chain protons in both compounds move steadily upfield. The only exceptions are Trp H2/H2′ (which

(46) Hasinoff, B. B.; Dunford, H. B.; Horne, D. G. *Can. J. Chem.* **1969**, *47*, 3225−3232.

(47) SPECFIT program version 2.11 (Spectrum Software Associates, Chapel Hill, NC).

(48) Benson, D. R.; Valentekovich, R.; Tam, S.-W.; Diederich, F. *Helv. Chim. Acta* **1993**, *76*, 2034−2060.

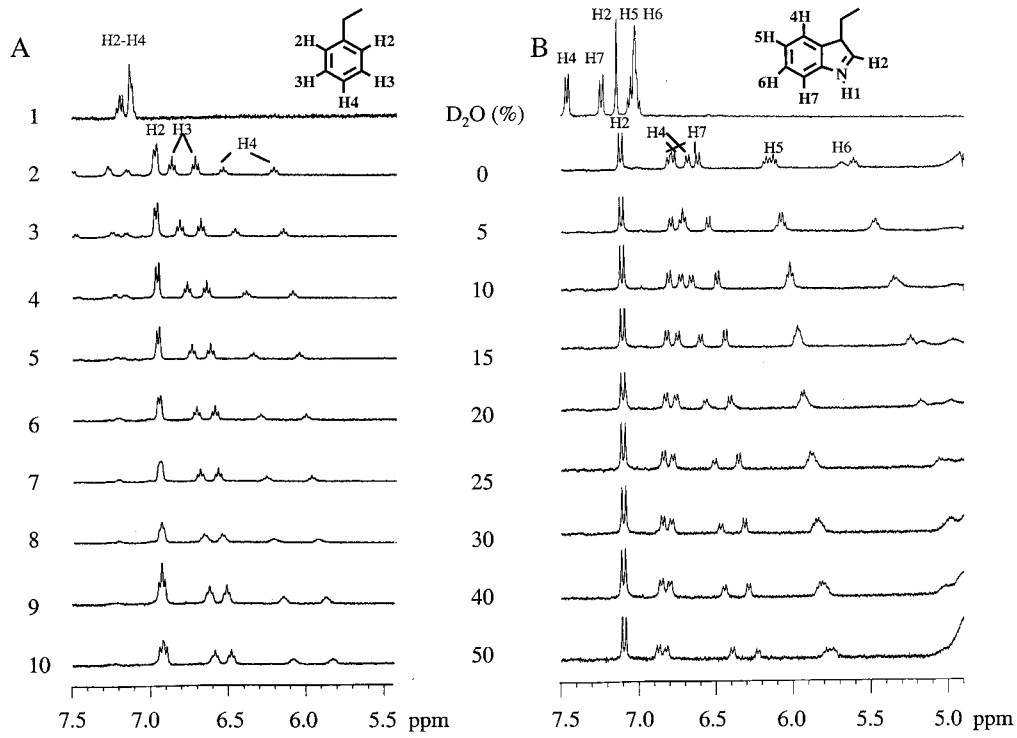

Figure 10. Regions of the NMR spectra of **2-Co** (A) and **3-Co** (B) and their peptide precursors. Spectra of the peptides were recorded in CD_3OD (Spectrum 1). Spectra of **2-Co** and **3-Co** were recorded in CD_3OD (spectrum 2) and with increasing volume percent of D_2O (spectra 3−10). Volume percent of D_2O is indicated in the center of the figure.

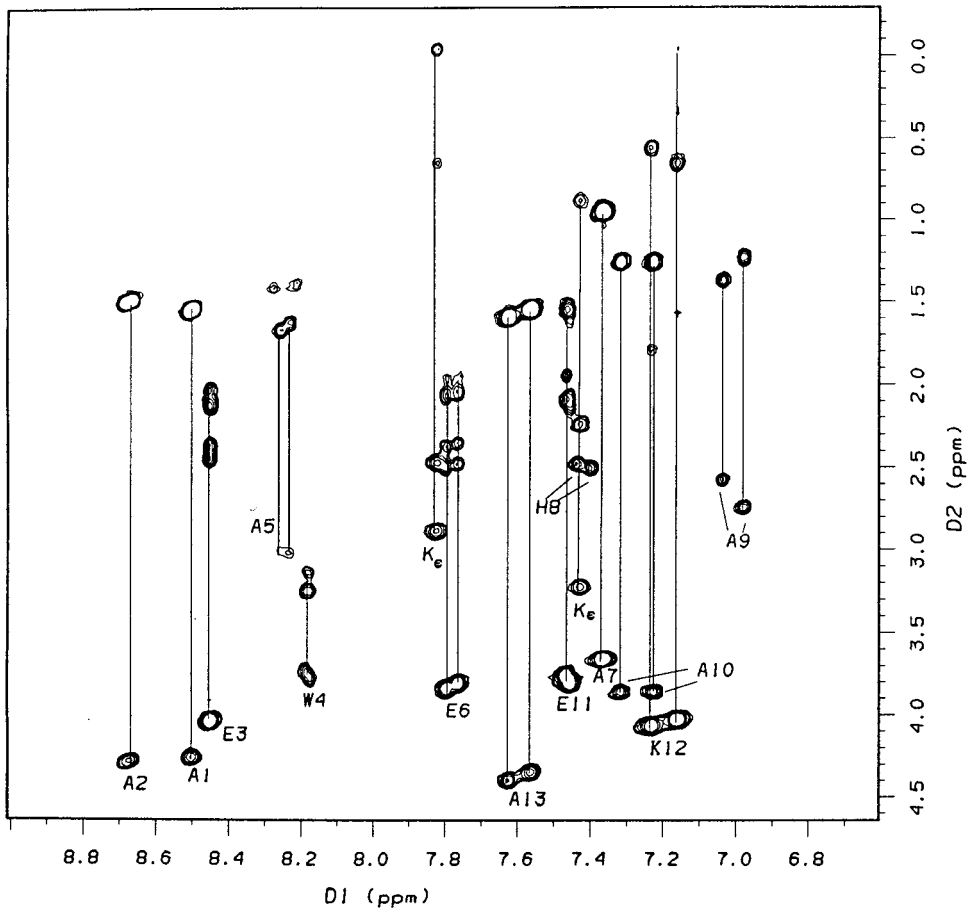

Figure 11. Fingerprint region of a HOHAHA spectrum of **3-Co** recorded in 1:1 CD_3OH/CD_3OD in 50 mM potassium phosphate buffer, pH 6.0, 23 °C.

are essentially unchanged) and H4/H4′, which actually move downfield (although in the end they are still upfield from their normal position). The pattern of the chemical shift changes indicate enhanced interactions between the side chains and the

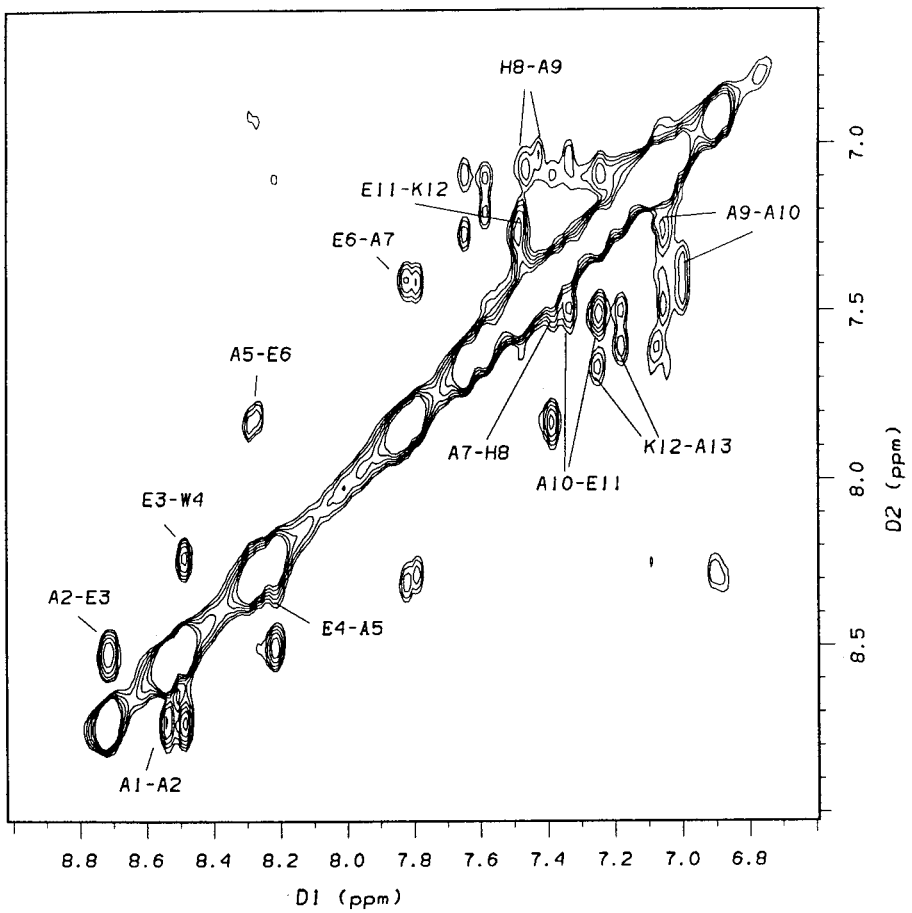

Figure 12. Amide−amide region of a 2D-NOESY spectrum of **3-Co** recorded in 1:1 CD_3OH/CD_3OD 50 mM potassium phosphate buffer, pH 6.0, at 23 °C.

porphyrin in more polar solvents, which results in more defined orientations between the chromophores. The observed solvent-dependent behavior is consistent with expectations for interactions driven primarily by hydrophobicity.

The relative shifts of the Trp side chain protons in **3-Co** are consistent with the helix orientation predicted in molecular modeling experiments (Figure 3) rather than the alternative structure[27b] in which the peptide helix axes are parallel to the porphyrin plane. In the predicted structure, the six-membered ring of the indole is closer to the porphyrin than the five-membered ring, and H6 and H7 are predicted to make van der Waals contact with the porphyrin. Correspondingly, Trp H6 undergoes the largest upfield shift (~2.2 ppm in 1:1 D_2O/CD_3OD), while H5 and H7 are both shifted upfield by more than 1 ppm in the same solvent. Although H7 is shifted upfield less than H5, it is predicted to reside near the edge of the porphyrin ring where ring current effects are at a minimum. H4 is the least shifted proton on the six-membered ring, commensurate with its greatest distance from the porphyrin. H1 and H2 show the smallest overall shifts, again in keeping with our model of **3** in which the five-membered ring of the indole is more distant from the porphyrin than the other ring. In the model, both of these protons point toward the solvent and are located beyond the rim of the porphyrin. If the peptides instead were oriented parallel to the porphyrin, the orientation of the Trp side chain required for van der Waals contact with the porphyrin would place the indole H1 and H7 protons in closest contact with the porphyrin ring, producing a chemical shift pattern very different from that observed.

All three side-chain protons in **2-Co** are shifted upfield relative to their positions in the monomeric peptide (Figure 10A). The largest shifts are for H4 (para) while the two indistinguishable H2 protons (ortho) are shifted the least. Although this pattern would be expected for both T-stacking and π-stacking arrangements, our model studies indicate that a π-stacking Phe−porphyrin arrangement would require a greater disruption of the peptide helix than would T-stacking and, thus, is less likely.

2D NMR Structural Studies. Two-dimensional (2D) NMR studies with **1-Co**, **2-Co** and **3-Co** have been performed in 1:1 CD_3OH/H_2O buffered to pH 6.0 with 50 mM potassium phosphate. This solvent was chosen to avoid self-association, which appears to occur in 3:1 H_2O/CH_3OH (the solvent used in most other studies in this report) at the 3 mM concentration desired for NMR experiments. Approximate helix contents in this solvent system as determined by CD are **1-Co** (63%), **2-Co** (68%), and **3-Co** (92%) (data not shown). The fingerprint region of the HOHAHA spectrum and the NH−NH region of the 2D-NOESY spectrum of **3-Co** are shown in Figures 11 and 12, respectively. The corresponding data for **1-Co** and **2-Co** are included with the Supporting Information. The His side chain protons in all three compounds are shifted characteristically upfield due to their location near the center of the porphyrin ring. These resonances served as useful starting points for assigning other signals in the spectrum, which was accomplished by standard methods.[49] The propionate groups of the porphyrin were identified from NOE cross-peaks with the Nϵ hydrogens of Lys 12 and 12′, and the remaining porphyrin protons were assigned using the NOE and HOHAHA data. Chemical shifts for all protons in **1-Co**, **2-Co** and **3-Co** are listed in Tables 3−5

(49) Wüthrich, K. *NMR of Proteins and Nucleic Acids*; Wiley: New York, 1986.

Table 3. Chemical Shifts and Coupling Costants for **1-Co**

residues	$^3J_{HN\alpha CH}$ (Hz)	NH	αH	βH	γH	δH	others
Ala1		8.44	4.20	1.48			
Ala2	5.46	8.62	4.20	1.45			
	5.51[a]	**8.60**	**4.19**	**1.45**			
Glu3	4.81	8.71	4.00	2.03	2.36, 2.29		
	5.12	**8.67**	**4.02**	**2.04**	**2.36, 2.29**		
Ala4	8.08	3.86	1.25				
	8.08	**3.84**	**1.22**				
Ala5	8.04	3.44	1.49				
	7.99	**3.52**	**1.45**				
Glu6		8.03	3.84	1.96	2.36, 2.27		
		7.99	**3.82**	**1.93**	**2.31, 2.23**		
Ala7		7.68	3.68	0.95			
		7.64	**3.66**	**0.89**			
His8		7.07	2.85	1.33			4H −0.70
		7.03	**2.88**	**1.32**			**−0.61**
							2H 0.25
							0.12
Ala9		7.04	2.73	1.26			
		6.97	**2.99**	**1.13**			
Ala10		7.53	3.85	1.25			
		7.57	**3.84**	**1.25**			
Glu11		7.52	3.82	1.60	2.01, 1.92		
		7.60	**3.86**	**1.70**			
Lys12	7.28	7.29	4.02	0.89, 1.52	0.42, 0.63	0.85, 0.30	NεH 7.72
	7.28	**7.29**	**4.02**	**0.74, 1.76**	**0.23, −0.19**	**0.89**	**7.54**
							Hε 2.73, 2.52
							3.16, 2.23
Ala13		7.59	4.28	1.50			

Porphyrin protons

$2\alpha CH_2$	- - - - -	$7CH_2$	4.03	$12\alpha CH_2$	- - - - -	$17CH_2$	4.05
$2\beta CH_2$	3.41, 3.17	$7CH_3$	1.84	$12\beta CH_2$	3.41, 3.17	$17CH_3$	1.76
$3CH_3$	3.72	$8CH_3$	3.68	$13CH_3$	3.73	$18CH_3$	3.72
5H	10.30	10H	10.49	15H	10.31	20H	10.53

[a] Bold-face numbers represent signals from one peptide, while light-face numbers represent those from other peptides. Where only one signal is observed, light-face type is used.

along with all coupling constants that could be determined from 1D spectra (insufficient resolution and strong signal overlap in DQF-COSY spectra prevented us from obtaining reliable coupling constants for the other amide hydrogens).

Figure 11 and Tables 3−5 reveal that most of the amino acids occupying identical positions on the two peptides of each Co(III) PSM have different chemical shifts for both backbone and side chain protons. This result once again demonstrates that the two peptides reside in slightly different chemical environments.

Sequential and short-range NOE connectivities used in secondary structure determination are shown in Figure 13 for **1-Co**, **2-Co,** and **3-Co**. Data are only shown for one of the two peptides in each compound. Connectivities that are obviously present but whose intensities could not be determined due to signal overlap are indicated by dashed lines. Signals that could not be observed but which might be obscured by signal overlap are indicated by dot−dash lines.

For **1-Co** and **3-Co**, NN(i, $i+1$) and αN(i, $i+1$) NOEs are detected from Ala-1 through Ala-13, save for the αN(i, $i+1$) signal between Lys-12 and Ala-13 in **3-Co**. For **3-Co**, the NN(i, $i+1$) signals are generally more intense than the αN(i, $i+1$) signals, which is typical for peptides having helical conformations.[49] In contrast, the NN(i, $i+1$) and αN(i, $i+1$) NOE signals in **1-Co** have similar intensities, suggesting that the helices in this this compound may have greater conformational flexibility than the helices in **3-Co**.

Even more characteristic of α-helical conformations are moderately strong αN(i, $i+3$) and αβ(i, $i+3$) NOEs, with the latter in general having greater intensity.[49] The αN(i, $i+3$) and αβ(i, $i+3$) NOE signal intensities for **1-Co** and **3-Co** are generally weaker (if not absent) near the N- and C-termini than near the peptide center. This suggests looser structural organization (fraying) at the peptide termini, a commonly observed feature of monomeric helices which arises from a lack of hydrogen bonding partners for the first and last several residues of the helix[50] (Ala-1 through Ala-3 and Glu-11 through Ala-13 in the present case). For **3-Co**, only the αN(i, $i+3$) signal between Ala-2 and Glu-5 and the αβ(i, $i+3$) signal between Ala-1 and Trp-4 are missing, and the relative αN(i, $i+3$) and αβ(i, $i+3$) signal intensities are as expected for helical conformations. A greater number of NOE signals characteristic of helicity are absent in **1-Co**, including two αN(i, $i+3$) interactions near the center of the peptide (Figure 13). Furthermore, the αN(i, $i+3$) signals of **1-Co** are generally more intense than the αβ(i, $i+3$) signals. These findings provide additional evidence that the helices in **1-Co** have greater conformational flexibility than those in **3-Co**, supporting the results of H/D exchange experiments on the Fe(III) analogues. The greater conformational flexibility in **1-Co** than in **3-Co** confirms the different average helix contents measured by CD.

For **2-Co**, αN(i, $i+3$) and αβ(i, $i+3$) NOEs are observed only from Phe-4 through Ala-13 (the Ala-2 to Ala-5 αβ(i, $i+3$) NOE connectivity was present when a mixing time of 300 ms was used, but was absent at both shorter and longer mixing times and thus is probably spurious). The αβ(i, $i+3$) signals are more intense than the αN(i, $i+3$) signals, and the NN(i, $i+1$) signals tend to be stronger than the αN(i, $i+1$) signals.

(50) Chakrabartty, A.; Baldwin, R. L. *Adv. Protein Chem.* **1995**, *46*, 141−176.

Table 4. Chemical Shifts and Coupling Costants for 2-Co

residues	$^3J_{HN\alpha CH}$ (Hz)	NH	αH	βH	γH	δH	others
Ala1		8.40	4.16	1.47			
Ala2		8.55	4.11	1.41			
Glu3		8.59	3.96	2.07, 1.99	2.35, 2.28		
Phe4		8.09	3.89	3.05, 2.94			2H 6.90
							6.89
							3H 6.54
							6.47
							4H 6.02
							5.87
Ala5		8.11	3.26	1.44			
		8.09[a]	**3.26**	**1.40**			
Glu6		7.81	3.73	1.94, 1.89	2.31, 2.25		
		7.79	**3.71**	**1.94, 1.89**	**2.31, 2.25**		
Ala7		7.48	3.62	0.90			
		7.47	**3.62**	**0.84**			
His8		7.37	2.61	0.97, 0.61			4H −0.56
	5.12	**7.45**	**2.51**	**0.97, 0.59**			**−0.73**
							2H 0.25
							0.19
Ala9		6.86	3.04	1.07			
		6.85	**2.93**	**1.19**			
Ala10		7.37	3.78	1.24			
Glu11		7.49	3.80	1.70	2.11		
Lys12		7.19	3.96	0.97, 1.47	0.28, 0.59	0.23, 0.57	Nϵ H 7.68
		7.16	**3.96**	**0.79, 1.56**	**0.45, 0.06**	**0.73, 0.57**	**7.57**
							Hϵ 2.49
							2.93, 2.50
Ala13		7.47	4.23	1.44			
		7.41	**4.16**	**1.40**			

Porphyrin protons

$2\alpha CH_2$	- - - - -	$7CH_2$	3.97	$12\alpha CH_2$	- - - - -	$17CH_2$	3.97
$2\beta CH_2$	3.37, 3.17	$7CH_3$	1.8	$12\beta CH_2$	3.34, 3.23	$17CH_3$	1.80
$3CH_3$	3.68	$8CH_3$	3.64	$13CH_3$	3.77	$18CH_3$	3.67
5H	10.30	10H	10.55	15H	10.31	20H	10.48

[a] Bold-face numbers represent signals from one peptide, while light-face numbers represent those from other peptides. Where only one signal is observed, light-face type is used.

These findings indicate that the helices in **2-Co**, although short, are well-organized. The near absence of NOE connectivities for the first three N-terminal residues of **2-Co** followed by a well-ordered short helix indicates that, rather than being frayed, the three N-terminal residues are devoid of helical character.

Although CD data suggested that peptide helix contents in **1** and **2** and their Co(III) analogues are similar, H/D exchange and pH titration experiments showed that the peptides have quite different properties. This difference is confirmed by the NMR data for **1-Co** and **2-Co** which reveal a nearly full-length, conformationally flexible helix in **1** and a shorter, less dynamic helix in **2**. This result highlights a problem inherent in using only CD data to compare structural properties of even closely related peptide helices, particularly when long-range interactions involving amino acid side chains are involved: helix contents obtained from CD represent the population of helical conformations averaged over all residues in the peptide, but provides no information as to how this population is distributed.

Structural Implications of Chemical Shift Patterns. Figures 14 and 15 show chemical shift indexes (CSIs) for the α-NH and α-CH hydrogens, respectively, in **1-Co**, **2-Co,** and **3-Co**. The value plotted for each residue represents the change of its chemical shift relative to the average chemical shift observed for the same amino acid in random coil peptides.[49] For helical peptides, one typically observes upfield shifts (negative CSIs) for α-NH protons and downfield shifts (positive CSIs) for α-CH protons.[51] Figures 14 and 15 reveal that most of the α-CH and α-NH protons exhibit large negative CSIs, a result of the large diamagnetic ring current of the porphyrin. The α-NH protons for residues Ala-1 through Glu-3 are shifted downfield from the positions expected for randomly oriented residues (the zero line in the figure), despite the fact that these residues are frayed or disordered in each structure. This observation suggests that the amide backbone hydrogens of residues 1−3 in all three compounds and of Trp-4 in **3-Co** are situated within the deshielding region of the porphyrin. The data further suggest that the peptide crosses the shielding/deshielding border near residues four and five. Significantly, in the predicted structures in which the peptides are fully helical, residues 1−3 extend beyond the edge of the porphyrin ring (Figure 3).

Focusing on the α-NH and α-CH CSIs for residues 4 and 5 (Figures 14 and 15), an interesting trend is observed: the magnitude of the upfield shift increases as the residue at position four is changed from Ala to Phe to Trp. In fact, at position four the Trp-4 α-NH CSI is positive, while the corresponding CSIs for Ala-4 and Phe-4 are negative. These data suggest that residues 4 and 5 are held more firmly in place near the porphyrin edge as residue four is changed from Ala to Phe to Trp. Between residue 6 and 13, the magnitude of the α-NH upfield shifts generally decrease in the order **3-Co**>**2-Co**>**1-Co**. This is consistent with a corresponding decrease in the strength of intrahelical hydrogen bonding but may also indicate that the location of each residue relative to the porphyrin is enforced the most in **3-Co** and the least in **1-Co**. Regardless of the degree to which these factors contribute to the chemical shift, it is clear that conformational flexibililty decreases in the order **1-Co** >

(51) Wishart, D. S.; Sikes, B. D.; Richards, F. M. *J. Mol. Biol.* **191**, *222*, 311−333.

Table 5. Chemical Shifts and Coupling Costants for **3-Co**

residues	$^3J_{HN\alpha CH}$ (Hz)	NH	αH	βH	γH	δH	others
Ala1	5.12	8.50	4.27	1.55			
Ala2	5.46	8.68	4.29	1.50			
Glu3	3.41	8.45	4.04	2.14, 2.06	2.44, 2.38		
Trp4		8.17	3.77	3.25, 3.15			2H 7.26
		8.19[a]	**3.75**	**3.25, 3.14**			7.25
							4H 6.90
							6.88
							5H 5.75
							5.76
							6H - - - - -
							7H 6.28
							6.35
							NH 9.69
							9.82
Ala5		8.24	3.02	1.63			
		8.26	**3.01**	**1.68**			
Glu6		7.77	3.81	2.05,1.96	2.49, 2.37		
		7.79	**3.85**	**2.06,1.98**	**2.50, 2.39**		
Ala7		7.36	3.66	0.95			
His8		7.40	2.50	0.65, −0.03			4H −0.59
		7.44	**2.48**	**0.63, −0.17**			−0.78
							2H 0.35
							0.35
							NH 9.51
							9.44
Ala9		6.98	2.75	1.24			
		7.03	**2.58**	**1.36**			
Ala10	5.46	7.33	3.87	1.26			
		7.22	**3.86**	**1.26**			
Glu11		7.47	3.77	1.55	1.96		
Lys12		7.16	4.04	0.56, 1.53	−0.04, 0.32	0.63	NεH 7.83
		7.22	**4.08**	**0.53, 1.77**	**−0.06**	**0.87**	7.43
							Hε 2.90, 2.49
							3.24, 2.24
Ala13	5.81	7.63	4.42	1.59			
	5.47	**7.57**	**4.36**	**1.55**			

Porphyrin protons

$2\alpha CH_2$	- - - - -	$7CH_2$	3.89	$12\alpha CH_2$	- - - - -	$17CH_2$	1.67
$2\beta CH_2$	3.40	$7CH_3$	1.81	$12\beta CH_2$	3.53, 3.33	$17CH_3$	4.02
$3CH_3$	3.68	$8CH_3$	3.75	$13CH_3$	3.91	$18CH_3$	3.69
5H	10.36	10H	10.74	15H	10.63	20H	10.78

[a] Bold-face numbers represent signals from one peptide, while light-face numbers represent those from other peptides. Where only one signal is observed, light-face type is used.

2-Co > **3-Co**, supporting the conclusions from the NOE data and the results of the H/D exchange studies of **1**−**3**.

The different effects of Trp and Phe on molecular architecture, the chemical shift pattern observed for the Trp side chains in **3-Co**, and the CSI data discussed above suggest strongly that the orientation of the peptide helices in **1**−**3** is similar to that predicted in molecular modeling studies. Periodicities observed in the α-CH and α-NH CSI data and differences in the chemical shifts of His-8 α-NH and β-hydrogens in **2-Co** and **3-Co** relative to **1-Co** provide additional compelling evidence for the validity of the model. The data for **1-Co** in Figure 14 show that the α-NH hydrogens of His-8 and Ala-9 have the largest upfield shifts. From molecular models, the distances beween Fe and the α-NH hydrogens of Ala-9 and His-8 are very similar, although the α-NH of Ala-9 is positioned more directly over the center of the porphyrin. Lys-12 is exactly one helical turn ahead of residues 8 and 9, and in the model its α-NH is situated closer to the porphyrin ring than any other α-NH (see model of **3** in Figure 3), but is also nearer the porphyrin edge than Ala-9 or His-8. Although Ala-5 is one helical turn to the C-terminal side of residues 8 and 9, its α-NH is only slightly upfield-shifted. The α-CH CSIs exhibit a different periodicity. Again the largest upfield shifts are for His-8 and Ala-9. However, the Ala-5 α-CHs are also significantly upfield-shifted while only very small negative CSIs are observed for the a α-CHs of Lys-12.

In helical peptides, the α-NH hydrogens and the side chains point in the direction of the N-terminus, while the α-CHs point toward the C-terminus. In the model of **3** (Figure 3), the α-NH of Lys-12 is thus oriented more toward the porphyrin shielding region than is the α-CH. The opposite is true for Ala-5; the α-CH is oriented more over the porphyrin shielding region than is the α-NH. Molecular models reveal that if the peptide helix axis were instead parallel to the porphyrin plane, the Ala-5 and Lys-12 α-NHs would be almost exactly the same distance from Fe and would have very similar orientations relative to the porphyrin (not shown). They would thus be likely to exhibit similar CSIs.

In **2-Co** and **3-Co**, the His-8 α-NH protons are not shifted as far upfield as the corresponding protons in **1-Co**. In addition, the two His-8 β-hydrogens of **2-Co** and **3-Co** exhibit quite different chemical shifts, and both signals are upfield-shifted relative to the single signal observed for the His-8 β-hydrogens of **1-Co** (these data are summarized in Table 6). Inspection of the model of **3** shows that the α-NH proton of His-8 resides near the edge of the Trp ring, and one of the β-hydrogens is positioned directly over the six-membered ring of the indole

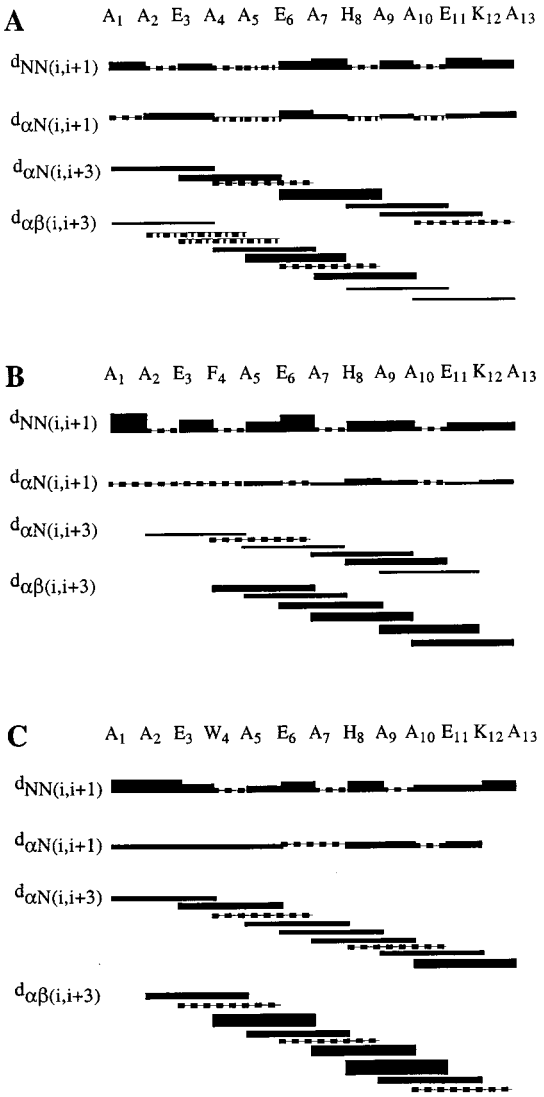

Figure 13. NOE connectivity diagrams of **1-Co** (A), **2-Co** (B), and **3-Co** (C). Relative signal intensities are indicated by line width. Signals which are present but whose intensities could not be determined due to signal overlap are indicated as dashed lines. Signals that are not observed but which might be obscured by signal overlap are indicated by dot−dash lines.

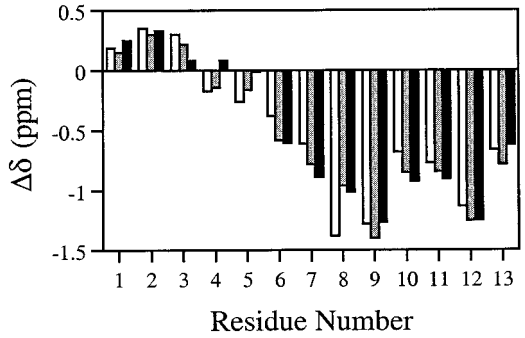

Figure 14. Chemical shift index of the α-NH hydrogens of **1-Co** (white), **2-Co** (gray), and **3-Co** (black). See text for details.

side chain. Such an orientation nicely explains the different chemical shifts of the His-8 α- and *β*-hydrogens in **3-Co** versus **1-Co**. The data for **2-Co** suggest that the Phe side chains adopt orientations similar to the Trp side chains in **3-Co**, indicating that it prefers T-stacking over *π*-stacking in the present system.

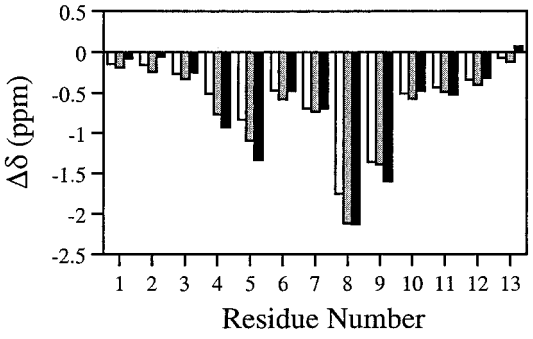

Figure 15. Chemical shift index of the α-CH hydrogens of **1-Co** (white), **2-Co** (gray), and **3-Co** (black). See text for details.

Table 6. Chemical Shifts of His-8 *β*- Hydrogens in **1-Co**, **2-Co** and **3-Co**

PSMs	*β*H	*β*′H
1-Co	1.33	- - - - -
	1.32[a]	
2-Co	0.97	0.61
	0.97	**0.59**
3-Co	0.65	−0.03
	0.63	**−0.17**

[a] Bold-face numbers represent signals from one peptide, while light-face numbers represent those from other peptides.

Conclusion

The ubiquitous occurrence of T-stacking and *π*-stacking interactions between aromatic amino acid side chains and heme in hemoproteins suggested that these interactions may have important roles in hemoprotein stability. In support of this hypothesis, we have demonstrated that the Phe and Trp side chains in **2** and **3** engage in strong nonbonded interactions with the covalently attached metalloporphyrin. Both interactions increase the stability of their respective model protein folds relative to **1**. When the side chain is sufficiently large, as is the case with Trp, stabilization of the peptide helix also results. The smaller side chain of Phe, in contrast, leads to a shorter helix. This short helix is more resistant to H/D exchange than the peptides in **1**, even though the average helix contents in **1** and **2** are quite similar. The similar helix contents of **1** and **2** are shown by NMR to result from different distributions of helix content throughout the peptide sequences.

Finally, data from NMR experiments provide compelling evidence that orientation of the peptide helices relative to the porphyrin plane in these model hemoproteins is similar if not identical to that predicted in molecular modeling studies. This result highlights the power of applying de novo design principles to the construction of protein-like molecules having well-defined structural characteristics.

Experimental Section

Reagents. All reagents were of commercial grade and were used without further purification except for dimethyl sulfoxide (DMSO), which was dried over 4 Å molecular sieves. Amino acids were purchased from either Advanced Chemtech (Louisville, KY) or Bachem (San Diego, CA). Rink resin was purchased from Advanced Chemtech (Louisville, KY). D_2O (99.9% D) was purchased from Aldrich (Milwaukee, WI), and CD_3OD (99.8% D) and CD_3OH (99.5% D) were as purchased from Cambridge Isotope Laboratories (Cambridge, MA).

Peptide Synthesis. Peptides were synthesized on a Rainin PS3 automated synthesizer using Fmoc chemistry[52] on Rink resin with (100−200 mesh, 1% DVB, substitution level 0.56−0.62 mmol/g),

(52) Fields, G. B.; Noble, R. L. *Int. J. Pept. Protein Res.* **1990**, *35*, 161−214.

followed by deprotection and cleavage from the resin using Reagent K.[53] Purification was achieved by HPLC (Rainin system HPLX) on a 2.2 cm Vydac C18 peptide/protein column using a gradient of acetonitrile in 0.1% TFA (5− 40% over 40 min) at a flow rate of 8 mL/min. Amino acid analyses for the peptide components of PSMs **2**−**3-Co** (**1** has already been reported) are as follows [AA, found (calcd)]. For **2** and **2-Co**: A, 7.28 (7); E, 2.76 (3); H, 0.97 (1); K, 0.99 (1); F, 1.01 (1). For **3** and **3-Co**: A, 7.33 (7); E, 2.67 (3); H, 1.01 (1); K, 1.00 (1); W, (1). For **1-Co**: A, 7.90 (8); E, 3.11, (3); H, 1.01, (1); K, 0.98, (1); p-fluoro-Phe (present). ESI MS: *m*/*z* (**2**/**2-Co**) 1356.8 (MH^+), (**3**/**3-Co**) 1395.6 (MH^+), (**1-Co**) 1374.9 (MH^+). All peptides were homogeneous as determined by analytical HPLC and by ESI-MS. Amino acid analyses were performed by the KU Biochemical Research Services Laboratory using FITC precolumn derivatization of peptides hydrolyzed in 6 M HCl (0.01% phenol) for 24 h.

Synthesis of 1−4. PSMs **1**−**4** were prepared from the bis (*p*-nitrophenyl) ester of iron(III) mesoporphyrin II[29a] and the appropriate peptide using the method previously reported for PSMs generated from iron(III) mesoporphyrin IX.[27b] ESI MS: *m*/*z* (**1**) 1049 ($M2H^{3+}$) (**2**) 1099.2 ($M2H^{3+}$), (**3**) 1125.2 ($M2H^{3+}$), (**4**) 1111.8 ($M2H^{3+}$)

Synthesis of 1-Co, 2-Co, and 3-Co. The peptide (50 uL of a 0.1 M solution) in dry DMSO was added to a solution of the bis-*p*-nitrophenyl ester of iron(III) mesoporphyrin II (10 uL of a 0.06 M solution) in 1:1 (v/v) pyridine/diisopropylethylamine. A solution of anhydrous Co-(OAc)2 (20 uL of a 0.23 M solution) was then added, and the mixture was vortexed for 4 h at room temperature. Once reaction was complete as determined by HPLC and UV/vis, 1 mL of 0.1 M NH_4OAc in 1:1 (v/v) H_2O/TFE was added. Sephadex CM-50 chromatography followed by reverse phase HPLC (Vydac 1.0 cm C4 peptide/protein column using a gradient of acetonitrile in 10 mM ammonium acetate, pH 5.8, 10−40% over 40 min at 2.0 mL/min) was used to purify the final product. ESI-MS: *m*/*z* (**1-Co**) 1049.7 ($M2H^{3+}$); (**2-Co**) 1100.3 ($M2H^{3+}$), (**3-Co**) 1126.3 ($M2H^{3+}$).

Circular Dichroism. CD experiments were performed on a JASCO 710 circular dichroism spectropolarimeter. The instrument is automatically calibrated with (1*S*)-(+)-10-camphosulfonic acid. Temperature control was achieved using a circulating water bath. For all studies, cell path length (*l*) was 1.0 cm. Concentrations of PSM stock solutions were determined by UV/vis spectroscopy, using an extinction coefficient of 130,000 M^{-1} cm^{-1} for **1**−**3** and of 180 000 M^{-1} cm^{-1} for the Co(III) analogues (discussed below). CD spectra in the far-UV region (190−250 nm) represent the average of 3−5 scans. Spectra in the far-UV are reported in terms of mean residue ellipticity ($[\theta]$, in deg·cm^2·$dmol^{-1}$), calculated as $[\theta] = [\theta]_{obs}(MRW/10lc)$ where $[\theta]_{obs}$ is the ellipticity measured in millidegrees, MRW is the mean residue molecular weight of the peptide (molecular weight divided by the number of amino acids), c = sample concentration in mg/mL, and l = optical path length of the cell in cm. Spectra in the Soret region are averages of 5−10 scans and are reported in terms of molar ellipticity ($[\theta]_{Soret}$, in deg·cm^2·$dmol^{-1}$), calculated as $[\theta] = [\theta]_{Soret}(MW/10lc)$ where MW is the molecular weight of the compound.

UV/vis Spectroscopy and Determination of PSM Extinction Coefficients. UV/vis spectra were recorded on a Kontron UVIKON 9410 recording spectrophotometer with a thermostated cell compartment using quartz cuvettes with a 1.0 cm path length. Extinction coefficients for **1**-**3** were determined as follows. The extinction coefficient of the bis-imidazole complex of iron(III) mesoporphyrin IX was measured in 1:1 ethanol/2.5 M imidazole and determined to be 139 000 M^{-1} cm^{-1}.[27a] Soret region UV/vis spectra of **1**−**3** were recorded under the same conditions and the sample concentration was determined using ϵ =139 000 M^{-1} cm^{-1} (in this solvent, the His ligands in **1**−**3** are replaced by imidazole as evidenced by absence of CD Soret signals). The spectrum of a sample at the same concentration in 50 mM potassium phosphate buffer, pH 7.0, was then recorded and the extinction coefficient was calculated. The extinction coefficient in each case is 130 000 M^{-1} cm^{-1}. For the Co(III) analogues, a CD spectrum of **3-Co** was first recorded in neutral aqueous solution. The concentration of the **3-Co** solution was calculated using the equation $[\theta] = [\theta]_{obs}(MRW/10lc)$ (see CD section, above) and the assumption that θ_{220} for **3** and **3-Co** is identical (the spectra are identical across the entire far-UV region). The extinction coefficient was measured by UV/vis using a sample at the same concentration. This extinction coefficient (180 000 M^{-1} cm^{-1}) was used for all three Co(III) PSMs.

pH Titrations. For pH titrations of **1**−**3**, sample concentrations ranged from 4 to 6 μM. The McIlvaine buffer system[54] (50 mM buffer in 3:1 (v/v) H_2O/CH_3OH) was used for data between pH 2.2 and 6.0. Buffers of pH lower than 2.2 were prepared by adjusting the pH of 50 mM citric acid with dilute HCl. pH measurements were made with an Accumet model 10 pH meter equipped with a silver chloride electrode and are uncorrected for MeOH content. All samples were thermostated at 23.0 °C. Data were fit using the program SpecFit.[47] For **2** and **3**, evidence of self-association appeared in samples at pHs below 2.5. To obtain fits of the data for **2** and **3**, we thus used the spectrum of **1** at pH 2.5 (**1** is completely unfolded at pH 2.5 and gives no evidence of self-association) to represent the completely unfolded forms of **2** and **3**.

Hydrogen/Deuterium Exchange Methods. Samples of **1**−**3** were lyophilized from stocks of known concentration and diluted into dry DMSO to produce 7.5 mM stock solutions. The infusion buffer consisted of 1:3 CD_3OD/D_2O with 2 mM ammonium acetate (pD* 6.2). A fully deuterated sample for use in determining the end point mass spectrum for each compound was prepared by mixing the DMSO stock solutions into the infusion buffer and allowing the solution to stand for at least 3 h.

Electrospray ionization (ESI) spectra were acquired on an AUTOSPEC-Q sector instrument equipped with a VG ESI source (VG Analytical Ltd, Manchester, UK). Voltage scans were acquired in continuum mode over a 30 amu window in 3.5 s. Samples were introduced from a 200 μL loop in a Rheodyne HPLC injector through a fused silica line (35 cm of 110 μM OD, 41 μM ID) threaded through the standard stainless steel needle (25 cm × 250 μM ID, 130 μM OD). Samples were diluted into the infusion buffer from a 7.5 mM DMSO stock to give a final concentration of 75 μM at 23 °C. After rapid mixing, the sample was injected into the loop. The initial flow rate was 20 μL/min and then reduced to 8 μL/min. The first data point was at 17 s or less. The ion monitored was $M2H^{3+}$.

Data from the $M2H^{3+}$ cluster was plotted according to eq 3 vs time in minutes, where ln(*Ht*) is the natural log of the number of unexchanged hydrogens remaining, $M2H^{3+}$ is the observed unresolved isotopic cluster, $M2D^{3+}$ is the fully exchanged unresolved isotopic cluster, and *t* is the time in minutes. Curve fittings of the decays were performed by the linear regression analysis method of Wagner et al.[44] yielding $r^2 > 0.98$ for all curve segments.

$$\ln(Ht) = \ln\{3[(M2D^{3+}) - (M2H^{3+})]\} \quad (3)$$

^{19}F NMR Data. Aqueous samples were prepared by dissolving **4** in a stock solution of 1 mM NaF/50 mM potassium phosphate buffer (pH 7.0). Samples at lower concentrations were obtained by diluting the initial sample with potassium phosphate buffer. Concentration of each sample was determind by UV/vis using the Soret signal at 403 nm (ϵ = 130 mM^{-1} cm^{-1}) after an appropriate dilution. Samples in 1:3 CH_3OH/50 mM phosphate buffer (pH 7.0) were prepared in the same fashion except that HLPC grade CH_3OH was used in preparation of the stock NaF/phosphate buffer. Dilutions of the methanol samples were made with 1:3 CH_3OH/50 mM phosphate buffer, pH 7.0. ^{19}F NMR spectra were acquired at room temperature on a Bruker AM-500 spectrometer (^{19}F operating frequency 470.599 MHz, 298 K). Each data set consisted of 32K points with a spectral window of 25,000 Hz. The data were referenced against an internal NaF standard. The data sets were processed in Felix 95.0 (MSI) using 0.5, 1, and 5 Hz of line broadening. The peak frequencies of **3-Co** were determined by peak fitting and averaged by processing data sets in triplicate. Computer fitting of the data was performed by thermal annealing of the data.

1D and 2D ^{1}H NMR Data. 1D and 2D ^{1}H NMR spectra were obtained using Bruker AM-500 and DRX-400 spectometers, and spectra were processed using Felix 95 (MSI, St. Louis). 2D spectra of **2-Co**

(53) King, D. S.; Fields, C. G.; Fields, G. B. *Int. J. Pept. Protein Res.* **1990**, *36*, 255−266.

(54) McIlvaine, T. C. *J. Biol. Chem.* **1921**, *49*, 183−186.

were taken using a 3 mM solution in CD_3OH/CD_3OD (1:1). The 1D solvent experiments were carried out at concentrations between 0.5 and 1 mM. Conventional pulse sequences were used for HOHAHA, NOESY, and DQF-COSY experiments. All 2D spectra were recorded in the time proportional phase incrementation (TPPI) method and were usually aquired with a spectral width of 1.0 kHz, 256 t_1 points, 2K data points in t_2 and 32 transients for each t_1 increment. Before Fourier transformation, the data were usually multiplied by shifted sine bell square in both t_2 and t_1. The water resonance was suppressed by continuous low-power irradiation at all times except during t_2. For HOHAHA experiments a typical mixing time of 70 ms was used. NOESY spectra were recorded with mixing times of 150 ms to 400 ms. NOE intensities were obtained from NOESY data recorded with a 300 ms mixing time. DQF-COSY spectra were collected over 2048 complex points with 112 transients for each of the 512 t increments. The spectral width was reduced to 7.0 kHz in the t_1 and t_2 dimensions.

Acknowledgment. This work was supported by NIH Grant R29-GM52431 (D.R.B.). The tandem MS was purchased with the aid of NIH Grant S10 RRO 6294-01 (T.D.W.) and the University of Kansas. The ESI source was purchased with support from NSF Grant CHE-9413975 (T.D.W.) and the University of Kansas. We thank Dr. Jim McCormick for assistance in fitting the pH titration data.

Supporting Information Available: CD spectra, H/D exchange data, and pH titration data for **1**−**3** and NMR data for **1-Co** and **2-Co**, (PDF). This material is available free of charge via the Internet at http://pubs.acs.org.

JA990606R